Am J Physiol Cell Physiol 299: C218–C229, 2010.
First published April 21, 2010; doi:10.1152/ajpcell.00383.2009.

oxLDL-induced decrease in lipid order of membrane domains is inversely correlated with endothelial stiffness and network formation

Tzu Pin Shentu,[1,2] Igor Titushkin,[2] Dev K. Singh,[1] Keith J. Gooch,[3] Papasani V. Subbaiah,[4] Michael Cho,[2] and Irena Levitan[1,2]

[1]*Pulmonary, Critical Care and Sleep Medicine, Department of Medicine, University of Illinois, Chicago, Illinois;* [2]*Department of Bioengineering, University of Illinois, Chicago, Illinois;* [3]*Department of Biomedical Engineering, Ohio State University, Columbus, Ohio; and* [4]*Department of Medicine, University of Illinois, Chicago, Illinois*

Submitted 25 August 2009; accepted in final form 6 April 2010

Shentu TP, Titushkin I, Singh DK, Gooch KJ, Subbaiah PV, Cho M, Levitan I. oxLDL-induced decrease in lipid order of membrane domains is inversely correlated with endothelial stiffness and network formation. *Am J Physiol Cell Physiol* 299: C218–C229, 2010. First published April 21, 2010; doi:10.1152/ajpcell.00383.2009.—Oxidized low-density lipoprotein (oxLDL) is a major factor in development of atherosclerosis. Our earlier studies have shown that exposure of endothelial cells (EC) to oxLDL increases EC stiffness, facilitates the ability of the cells to generate force, and facilitates EC network formation in three-dimensional collagen gels. In this study, we show that oxLDL induces a decrease in lipid order of membrane domains and that this effect is inversely correlated with endothelial stiffness, contractility, and network formation. Local lipid packing of cell membrane domains was assessed by Laurdan two-photon imaging, endothelial stiffness was assessed by measuring cellular elastic modulus using atomic force microscopy, cell contractility was estimated by measuring the ability of the cells to contract collagen gels, and EC angiogenic potential was estimated by visualizing endothelial networks within the same gels. The impact of oxLDL on endothelial biomechanics and network formation is fully reversed by supplying the cells with a surplus of cholesterol. Furthermore, exposing the cells to 7-ketocholesterol, a major oxysterol component of oxLDL, or to another cholesterol analog, androstenol, also results in disruption of lipid order of membrane domains and an increase in cell stiffness. On the basis of these observations, we suggest that disruption of lipid packing of cholesterol-rich membrane domains plays a key role in oxLDL-induced changes in endothelial biomechanics.

angiogenesis; cholesterol; sphingomyelin; lipid packing

OXIDIZED LOW-DENSITY LIPOPROTEIN (oxLDL) is well known to be accumulated in atherosclerotic lesions (48), and the level of oxLDL increases with hypercholesterolemia both in animal models of atherosclerosis (20, 21) and in humans (7, 42). Multiple studies have shown that exposure to oxLDL results in endothelial dysfunction, including impairment of nitric oxide (NO) release (2), disruption of the endothelial barrier (14), and decrease in endothelial cell (EC) migration (32). Our studies focus on elucidating the impact of oxLDL on endothelial biomechanics and on the role of endothelial biomechanics in control of angiogenesis.

Our earlier studies have shown that exposure to oxLDL significantly increases endothelial stiffness and facilitates the ability of endothelial cells to generate force (6). Furthermore, we have shown that endothelial cells freshly isolated from aortas of hypercholesterolemic pigs are significantly stiffer than cells isolated from aortas of control animals, indicating that diet-induced hypercholesterolemia results in significant changes in endothelial biophysical properties (6). Moreover, oxLDL-induced increase in endothelial stiffness and force generation is associated with an increase in the ability of the cells to elongate and form endothelial networks in a three-dimensional (3D) assay of angiogenesis (6). Indeed, the association between the ability of endothelial cells to generate force and EC network formation has been shown in earlier studies across multiple types of endothelial cells (18, 37, 43). A key question remains: can the impact of oxLDL on endothelial biomechanics be attributed to changes in membrane cholesterol or to other pathways, such as oxLDL-induced hydrolysis of sphingomyelin. In our previous studies, we have shown that oxLDL-induced endothelial stiffening can be simulated by cholesterol depletion induced either by a well-known cholesterol acceptor, methyl-β-cyclodextrin (MβCD), or by serum starvation (6). These observations were surprising and unexpected because, in artificial membranes, cholesterol removal is known to decrease membrane stiffness (12, 33). We have also shown, however, that cholesterol depletion increases the rigidity of the plasma membrane in endothelial cells and enhances membrane-cytoskeleton adhesion (40). The role of cholesterol in oxLDL-induced endothelial stiffening and morphogenesis, however, still remains controversial. Alternatively, since oxLDL was shown to induce activation of sphingomyelinases (SMase) and hydrolysis of sphingomyelin (1, 45), a second major component of cholesterol-rich membrane domains (3), effects of oxLDL on endothelial biomechanics might also be mediated by the activation of endothelial SMases. In this study, we discriminate between these possibilities and extend our studies to test the impact of oxLDL on lipid packing of the membrane.

Specifically, we use Laurdan two-photon imaging, a novel approach to elucidate lipid order of different membrane domains (11), to determine how oxLDL affects lipid packing of endothelial membranes. This method was used earlier to assess local membrane properties in both model membranes (11) and in live as well as fixed cells (15, 16). Our observations show that exposure to oxLDL results in significant shift in lipid packing of ordered membrane domains to a less ordered state. Furthermore, we also show that oxLDL-induced endothelial stiffening, an increase in force generation, and network formation are fully reversible by supplying cholesterol surplus but are not affected by sphingomyelin hydrolysis. We conclude, therefore, that oxLDL-induced changes in endothelial biome-

Address for reprint requests and other correspondence: I. Levitan, Pulmonary, Critical Care and Sleep Medicine, Dept. of Medicine, Univ. of Illinois at Chicago, 840 South Wood St. (Room 920-N CSB) Chicago, IL 60612-7323 (e-mail: levitan@uic.edu).

chanics critically depend on the distribution of membrane cholesterol and cholesterol-rich ordered membrane domains.

MATERIALS AND METHODS

Cell culture and reagents. Bovine aortic endothelial cells (BAECs; Cambrex, East Rutherford, NJ) were grown between *passages 5* and *20* in DMEM (Invitrogen, Carlsbad, CA) containing 10% fetal bovine serum (Sigma-Aldrich, St. Louis, MO), 10 μg/ml penicillin, streptomycin, and kanamycin sulfate (Invitrogen). Cell cultures were maintained in a humidified incubator at 37°C, with 5% CO_2. Cells were split every 3–4 days. oxLDL (Biomedical Technologies, Stoughton, MA) was dissolved in DMEM medium to a final concentration of 10 μg/ml, and thiobarbituric acid-reactive substances were assayed as a measure of oxidative lipid modification (18–26 nmol malondialdehyde/mg protein). MβCD, cholesterol, and sphingomyelinase C (SMase C) from *Staphylococcus aureus* were purchased from Sigma Chemical (St. Louis, MO). 7-Keto-cholesterol and androstenol were purchased from Steraloids (Newport, RI). MβCD saturated with cholesterol was prepared as described previously (26).

Laurdan multiphoton microscopy. Analysis of the physical properties of ordered and disordered membrane domains was performed using a Laurdan two-photon microscopy, as described earlier (15, 17). Briefly, the images were acquired with a Bio-Rad multiphoton microscope. Cells were loaded with 5 μm Laurdan dye (Molecular Probes, Carlsbad, CA) in serum-free medium with DMSO used as a vehicle as described earlier (15, 17). Laurdan fluorescence was excited with a mode-locked titanium-sapphire laser with the multiphoton laser excitation set at 800 nm. The images were obtained with ×63 oil immersion objective (1.3 numerical aperture). The emitted light was collected in the ranges 410–490 and 503–553 nm. The general polarization was calculated using the equation:

$$GP = \frac{I_{(410-490)} - I_{(503-553\ nm)}}{I_{(410-490)} + I_{(503-553\ nm)}} \quad (1)$$

Here, general polarization (GP) values were corrected using the G-factor obtained for Laurdan in DMSO (stock solution 500 μm) for each experiment as listed below:

$$GP = \frac{I_{(410-490)} - G \times I_{(503-553\ nm)}}{I_{(410-490)} + G \times I_{(503-553\ nm)}} \quad (2)$$

G-factor is calculated through two variables: GP_{theo} and GP_{exp}. GP_{theo} is a known GP value for the Laurdan in DMSO at 22°C, and GP_{exp} is determined experimentally from GP value of the stock solution (500 μm) at room temperature. The equation is shown as

$$G = \frac{GP_{theo} + GP_{theo} \times GP_{exp} - 1 - GP_{exp}}{GP_{theo} \times GP_{exp} - GP_{theo} + GP_{exp} - 1} \quad (3)$$

GP images (512 × 512, 32 bits) were analyzed and pseudocolored in ImageJ software (NIH Image, National Institutes of Health, Bethesda, MD). The threshold was set to 90% coverage of the pixel values of combining the image [$I_{(410-490)} + I_{(503-553\ nm)}$]. Background values were set to zero. The GP distribution was obtained from the average histogram of 23–25 images, normalized (sum = 10,000), and fitted into two Gaussian distributions by using nonlinear fitting algorithm (Microsoft Excel). The data did not allow an unambiguous separation into more than two populations. The same limitation was noted previously (15). The general range of the GP values is between −1 and +1, with higher values corresponding to the higher order in the membrane. In the earlier studies, lipid ordered/raft domains were found in the range of $0.25 < GP < 0.55$ with disordered domains appearing in the range of $0.05 < GP < 0.25$ (15, 16). In liposomes with equal molar ratios of dioleoylphosphatidylcholine, cholesterol, and sphingomyelin, the range was somewhat different with $GP > 0.55$ and $GP < -0.05$ representing membranes in gel and fluid phase, respectively (11). In our study, however, we see a separation between more ordered and less ordered domains with the GP values of $0 < GP < 0.6$ and $-0.6 < GP < 0$, respectively. While the difference between our study and previous studies in the absolute GP values is not exactly clear, the most important observation is that not only is there a clear separation between less and more ordered domains but also that both cholesterol depletion and oxLDL induce significant shift from more ordered to less ordered states.

Cholesterol esterification (acyl-CoA:cholesterol acyltransferase) and cholesterol efflux assays. Acyl-CoA:cholesterol acyltransferase (ACAT) activity in intact cells was measured by the conversion of labeled cholesterol to cholesteryl esters as described previously (39). Briefly, the cells were labeled in six-well (35 mm) plates with [^{3}H]cholesterol by incubation with 0.1 μCi of labeled cholesterol complexed with 20% MβCD (final concentration of MβCD, 0.05%) for 10 min at room temperature. After removal of the labeling buffer and rinsing of the cell monolayer with DMEM, 5% lipoprotein-deficient serum in DMEM containing was added to each well, and incubated for 2 h at 37°C in the presence LDL (10 μg/ml) or oxLDL (10 μg/ml) or SMase C (0.025 μg/ml). The cells were then trypsinized, transferred to glass tubes, and extracted with 5 ml of chloroform:methanol (2:1 vol/vol). The chloroform extract was separated on silica gel thin layer chromatography plate with the solvent system of hexane:ethyl acetate (90:10 vol/vol), and the radioactivity in cholesterol and cholesteryl ester spots was determined in a liquid scintillation counter. The percentage of cholesterol esterified was calculated from the radioactivity values. For cholesterol efflux assay, cells were labeled as described above, and cells were incubated for 2 h or up to 24 h with LDL (10 μg or 20 μg/ml) or oxLDL (10 μg or 20 μg/ml). The measurement of cholesterol efflux was determined as described previously (38).

Atomic force microscopy microindentation. Elastic modulus of individual endothelial cells was measured with a Novascan atomic force microscope (Novascan Technologies, Ames, IA), as described previously (41). Briefly, cantilevers with borosilicate glass beads (10-μm diameter, 0.12 N/m) (Novascan Technologies) served as cell indentors. The atomic force microscopy (AFM) cantilever probe was positioned above the cell between the nucleus and the cell edge, and each cell was mechanically probed at five different locations, three times at each location avoiding the perinuclear and the edge regions. A total of 50–80 cells were analyzed for each experimental condition (15 force-distance curves acquired from each cell). The force curves were obtained by measuring the cantilever deflection at every vertical *z*-position of the cantilever as it approached and indented the cell. The cantilever descended toward the cell at a velocity of 2 μm/s until a trigger force of 3 nN was reached, which corresponded to 0.5–1 μm indentation depth, or approximately 10–15% of the total cell height. The force-distance curves were collected and analyzed according to the Hertz model:

$$F = \frac{4}{3}\frac{E}{(1-\nu^2)}\delta^{3/2}\sqrt{R} \quad (4)$$

where F is the loading force, δ is indentation depth, ν is the cellular Poisson's ratio (assumed to be 0.5), R is the radius of the spherical indentor (5 μm), and E is the local Young's elastic modulus. The bidomain polynomial model was fit to the experimental force curve using a standard least-squares minimization algorithm. The data are presented as histograms of the elastic moduli for each experimental condition. Statistical significance was calculated using a standard *t*-test ($P < 0.05$).

Preparation of gels and visualization of embedded endothelial cells. Collagen gels were prepared according to manufacturer's instructions to final collagen concentration of 1.5 mg/ml (Becton Dickinson, Franklin Lanes, NJ). BAECs were seeded into gel mixtures at $6–8 \times 10^5$/ml, and gels were allowed to polymerize for 20 min at 37°C in 48-well plates. Thereafter, the gels were mechanically loos-

ened from the sides of the wells, and growth media were supplemented with vascular endothelial growth factor (VEGF), basic fibroblast growth factor (bFGF), and phorbol myristate acetate (PMA) at concentrations of 50 μg/ml each. VEGF was obtained from Pepro Tech (Rocky Hill, NJ), and bFGF and PMA were obtained from Sigma. Gels were cultured for 48 h and gel contraction was quantified using MetaVue (Molecular Devices, Union City, CA). To visualize the cells, gels were fixed in 4% paraformaldehyde at 4°C overnight and stained with 0.1% toluidine blue (5 min). Images were obtained at ×10 magnification (Nikon, Eclipse TE200-U) to observe EC networks and analyzed using Scion Image as described previously (37). Four gels were analyzed for each condition in each individual experiment. At least three independent experiments were performed for each condition.

Statistic analysis. Statistical significance was evaluated using a standard *t*-test assuming two-tailed distributions with unequal variance.

RESULTS

oxLDL induces a decrease in lipid order of membrane domains. Cholesterol distribution is generally believed to define the lateral organization of the cell membrane into ordered (cholesterol-rich) and disordered (cholesterol-poor) membrane domains. Here, we use Laurdan two-photon microscopy to analyze the impact of oxLDL on the distribution and physical properties of ordered and disordered domains in endothelial cells. The general principle of the technique is that Laurdan is sensitive to the polarity of the local environment and undergoes a red shift as the phase boundary changes from gel to fluid (15, 17). Several earlier studies have used this approach to visualize ordered and disordered domains in both liposomes and cells (11, 15). As described earlier, changes in membrane order are estimated by calculating GP ratio, a normalized ratio of fluorescence intensity at 410–490 nm range (gel phase) and 503–553 nm range (fluid phase).

Figure 1 shows typical GP images for control cells, MβCD-treated cells, and cells exposed to oxLDL or oxLDL followed by MβCD-cholesterol. All images are shown in pseudocolor with yellow and red corresponding to the higher GP values, presumably ordered domains, and green and blue corresponding to the lower GP values, presumably disordered domains. Similarly to previous studies (15, 16), each cell has a punctate distribution of ordered and disordered domains throughout the entire surface of the cells under all experimental conditions. It is interesting to note, though, that ordered domains were concentrated in cell periphery (Fig. 1*A*). As expected, exposing cells to MβCD results in a shift to less ordered membrane structure, as indicated by a relative decrease in highly ordered (yellow) domains and an increase in less ordered (blue-green) domains. Most importantly, exposure to oxLDL also resulted

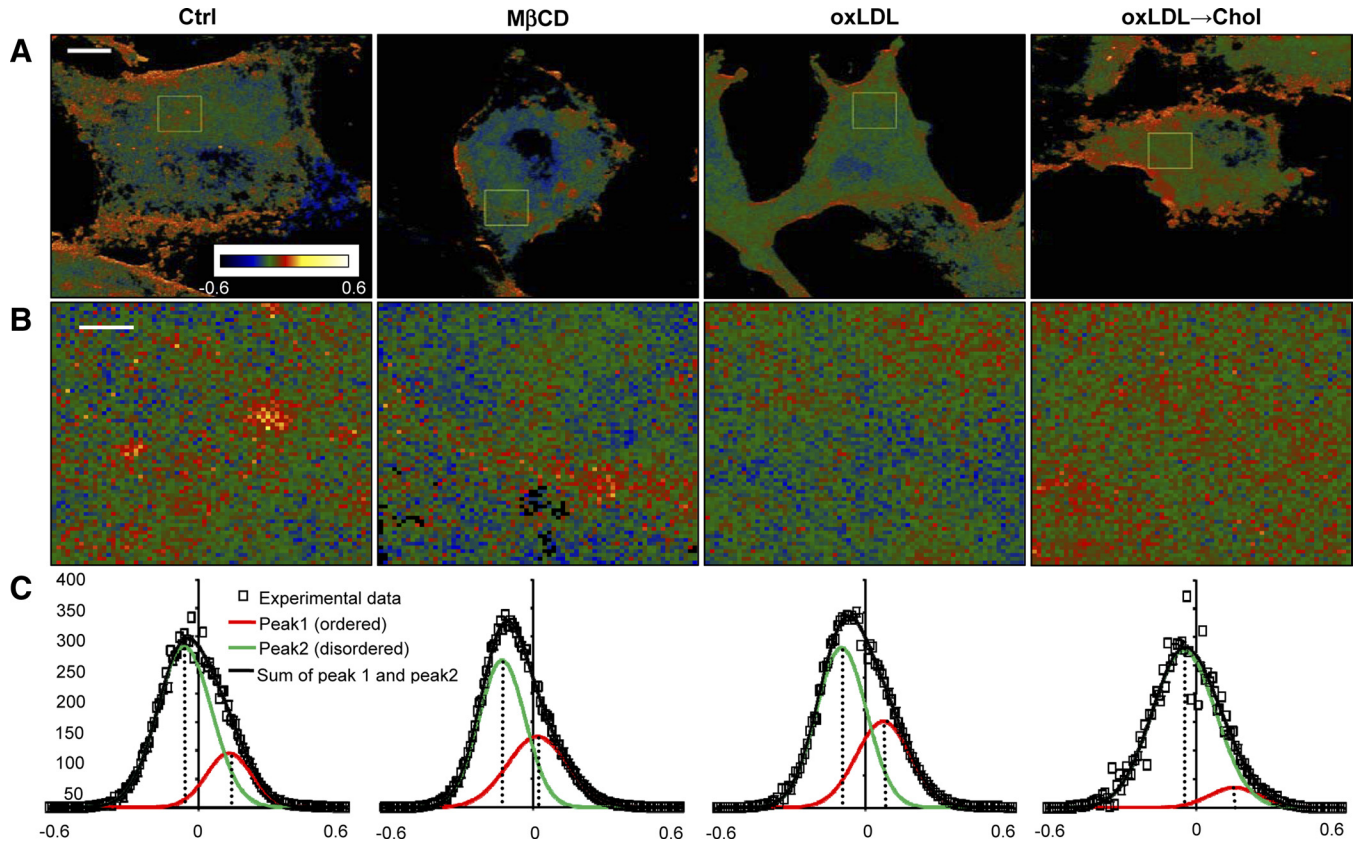

Fig. 1. Impact of oxidized low-density lipoprotein (oxLDL) on lipid packing of membrane domains in bovine aortic endothelial cells (BAECs). *A*: typical general polarization (GP) images of control cells (Ctrl), methyl-β-cyclodextrin (MβCD)-treated cells, oxLDL-treated cells (oxLDL), or cells exposed to oxLDL and MβCD-cholesterol sequentially (oxLDL→Chol). Scale bar is 5.6 μm. *B*: zoom-in representative regions of the GP images shown in *A* (the zoomed regions are 5.6 μm × 5.6 μm). Scale bar is 1 μm. *C*: GP histograms for the four experimental cell populations (dots) fitted by a two-Gaussian distribution with the curve shifted to the *right* representing ordered domains (red) and the curve shifted to the *left* representing fluid domains (green). The sum of the Gaussians is shown in black. GP distribution is obtained from the region −0.6 to +0.6 as shown in the *x*-axis, and the number of counts is normalized (sum = 10,000) as shown in the *y*-axis (n = 23–25 images per experimental condition, 4 independent experiments).

Table 1. *Analysis of the GP distributions for control, MβCD, oxLDL, and oxLDL/cholesterol-treated cells*

	Control	MβCD	oxLDL	oxLDL + Cholesterol
GP value				
Peak 1	0.09 ± 0.01	0.03 ± 0.01*	0.05 ± 0.02*	0.10 ± 0.02
Peak 2	−0.06 ± 0.01	−0.12 ± 0.01*	−0.08 ± 0.01	−0.06 ± 0.01
General GP	−0.02 ± 0.01	−0.08 ± 0.01*	−0.04 ± 0.01	−0.03 ± 0.02
%Coverage				
Peak 1	31 ± 4	33 ± 3	38 ± 5	22 ± 4
Peak 2	69 ± 4	67 ± 3	62 ± 5	78 ± 4

All values are means ± SE calculated from 23–25 images per condition obtained in 4 independent experiments. General polarization (GP) values for *peak 1* represent the mean order for the ordered domains, and GP values for *peak 2* represent the mean order of the fluid domains. The general GP values represent the overall order of the membrane. %Coverage shows the relative areas associated with each of the peaks representing each type of the domains. All experimental conditions were assayed on the same days. MβCD, methyl-β-cyclodextrin; oxLDL, oxidized low-density lipoprotein. *$P < 0.05$.

in a shift to less ordered membrane structure, as indicated by a loss of highly ordered (yellow) domains. However, replenishing membrane cholesterol of oxLDL-treated cells with MβCD-cholesterol partially reverses the effect.

Analysis of the GP distributions provides further insights into the impact of oxLDL on membrane structure. The histograms of the GP values for the four experimental cell populations were calculated from 23–25 images, each containing 1–5 cells, per condition and fitted with a two-Gaussian distribution with two peaks that are believed to represent ordered (peak with higher GP values) and disordered (lower GP values) membrane domains, as described in the earlier studies (15, 16). Furthermore, analysis of the GP values allows estimating the relative order of each type of the domains. Specifically, exposure to MβCD resulted in a decrease in peak values/lipid order of both ordered (red curve: 0.09 ± 0.01 vs. 0.03 ± 0.01 for control and MβCD-treated cells, respectively) and disordered domains (green curve −0.06 ± 0.01 vs. −0.12 ± 0.01 for control and MβCD-treated cells, respectively), indicating that, as expected, cholesterol depletion decreases lipid packing of the membrane (both peaks shift to the left; also see Table 1). The areas under the two peaks, however, do not change significantly, as was shown previously (15).

More surprisingly, exposure to oxLDL also results in a decrease in lipid packing. In this case, however, the effect is observed only for the ordered domains, as indicated by a shift in *peak 1* GP value (red curve: 0.09 ± 0.01 vs. 0.05 ± 0.02 for control and oxLDL-treated cells, respectively). Indeed, it is apparent from the relative positions of the peaks that both MβCD and oxLDL induce significant shifts of the GP values of the ordered domains to a less ordered state (also see Table 1). At the same time, the areas of the peaks which correspond to %membrane coverage of the domains relative to the whole membrane do not change significantly (Table 1). This is not completely unexpected, though, because earlier studies by Gaus et al. (15) have already shown that cholesterol depletion affects mainly the GP values of the peaks, not the peak areas. Thus, both studies are consistent in suggesting that removing cellular cholesterol alters the properties of the lipid domains rather than the degree of membrane coverage. Thus, analysis of the GP values shows that oxLDL decreases lipid packing of membrane ordered domains, an effect similar to that of MβCD exposure (Fig. 1*C* and Table 1). Conversely, replenishing membrane cholesterol by exposing oxLDL-treated cells to MβCD-cholesterol partially reverses the effect of oxLDL by increasing membrane order in a portion of membrane domains. Indeed, the peak GP value for the ordered domains in cells sequentially exposed to oxLDL and MβCD-cholesterol shifts to higher value compared with cells exposed to oxLDL alone and becomes very similar to that in control cells (0.09 ± 0.01 vs. 0.05 ± 0.02 vs. 0.1 ± 0.02 in control, oxLDL, and oxLDL + MβCD-cholesterol-treated cells, respectively). The area under the peak, however, is smaller than in control cells, suggesting that only a portion of membrane domains are recovered. These observations show that oxLDL decreases lipid order preferentially in the ordered domains and that this effect can be partially reversed by supplying cholesterol. We also tested the effect of cholesterol enrichment on control cells. In this case, both the general GP values and the GP values in both *peak 1* and *peak 2* increase, suggesting that the cholesterol enrichment, as expected, tightens lipid packing in both types of the domains (Table 2 and supplemental Fig. S1; Supplemental Material for this article is available online at the Journal website).

oxLDL facilitates cholesterol efflux. A decrease in lipid order induced by oxLDL and the reversal of the effect upon

Table 2. *Analysis of the GP distributions for control, cholesterol, 7-keto-cholesterol, and androstenol-treated cells*

	Control	Cholesterol	7-Keto-Cholesterol	Androstenol
GP values				
Peak 1	0.14 ± 0.01	0.17 ± 0.02*	0.09 ± 0.02*	0.05 ± 0.02*
Peak 2	−0.05 ± 0.01	0 ± 0.02*	−0.05 ± 0.02	−0.07 ± 0.01
General GP	0.03 ± 0.02	0.07 ± 0.02*	−0.01 ± 0.02	−0.01 ± 0.01
%Coverage				
Peak 1	46 ± 5	44 ± 5	43 ± 5	55 ± 4
Peak 2	54 ± 5	56 ± 5	57 ± 4	45 ± 4

All values are means ± SE calculated from 18 images per condition obtained in 3 independent experiments. The GP values represent membrane order and %coverage represents the relative areas of the ordered and fluid domains as described in Table 1. All experimental conditions were assayed on the same days. *$P < 0.05$.

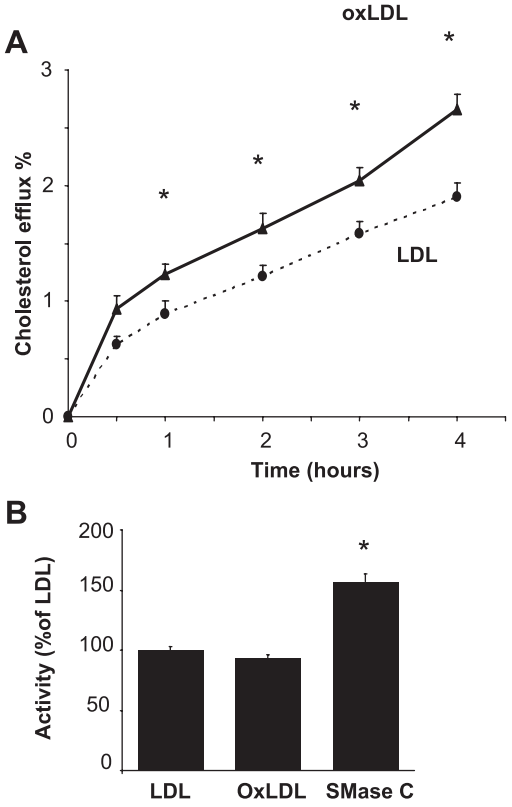

Fig. 2. oxLDL increases cholesterol efflux and has no effect on cholesterol esterification [acyl-CoA:cholesterol acyltransferase (ACAT)]. *A*: time courses of cholesterol efflux of endothelial cells exposed to LDL or to oxLDL (20 μg/ml). The values are means ± SE of three separate experiments normalized to control (LDL) (*$P < 0.05$). *B*: ACAT activity in 10 μg/ml LDL-, 10 μg/ml oxLDL-, and 0.025 U/ml sphingomyelinase C (SMase C)-treated cells ($n = 3$, *$P < 0.05$). Treating cells with SMase C (0.025 U/ml) increased the esterification of membrane free cholesterol about 1.6-fold, providing a positive control to cholesterol esterification assay. The values shown are means ± SE of three separate experiments.

addition of cholesterol suggest that oxLDL may facilitate cholesterol efflux. To test this possibility, we compared the time courses of cholesterol efflux from endothelial cells exposed to either oxLDL or LDL. In this series of experiments, we show that oxLDL facilitates cholesterol efflux and that statistically significant difference is observed already after 1 h (Fig. 2*A*). These observations are consistent with the earlier studies showing oxLDL-induced cholesterol efflux from endothelial caveolae (2). oxLDL-induced increase in cholesterol efflux is relatively small but it may result in significant changes in local lipid packing of cholesterol-rich domains, consistent with our observations shown above.

Since in our previous study we have shown that oxLDL induces internalization of G_{M1}, a major lipid raft marker (6), we proposed that oxLDL may also induce internalization of cholesterol from plasma membrane to the intracellular compartments. Earlier studies have shown that the degree of cholesterol internalization can be estimated by measuring the amount of newly formed cholesteryl ester because translocation of cell surface cholesterol that exists in free cholesterol form to the endoplasmic reticulum is accompanied by its esterification (38, 39). To test whether exposure to oxLDL facilitates cholesterol internalization, cells were pulse-labeled with [^{3}H] free cholesterol and exposed to 10 μg/ml protein oxLDL for 1 h as described above (LDL was used as control). In contrast to our expectations, however, oxLDL had no effect on the amount of labeled cholesteryl ester formed (Fig. 2*B*). Exposing the cells to SMase C was used as a positive control because it was shown earlier that a decrease in the level of sphingomyelin in the membrane results in internalization of cholesterol (38). Similar to the previous studies performed in macrophages, exposure of endothelial cells to SMase resulted in a significant increase in ACAT activity, but since total level of ACAT activity in endothelial cells is very low with only 2–3% cholesterol being esterified to cholesteryl ester, this treatment did not significantly affect the level of free cholesterol on the membrane.

Cholesterol reverses oxLDL-induced increase in endothelial elastic modulus. Consistent with our previous findings, we show here that exposure to oxLDL results in a clear shift in the distribution of the elastic modulus to higher stiffness (compare the histograms of the elastic modulus in Fig. 3, *Aa* and *Ab*), while unmodified LDL had no effect on the EC stiffness (not shown). To test the reversibility of oxLDL-induced effect on endothelial stiffening, cells were sequentially exposed first to oxLDL and then to MβCD-cholesterol. After the sequential oxLDL/MβCD-cholesterol exposure, the peak of the distribution becomes narrower, similar to control cells, and the values shift to lower elastic modulus (Fig. 3*Ac*). In addition, there is

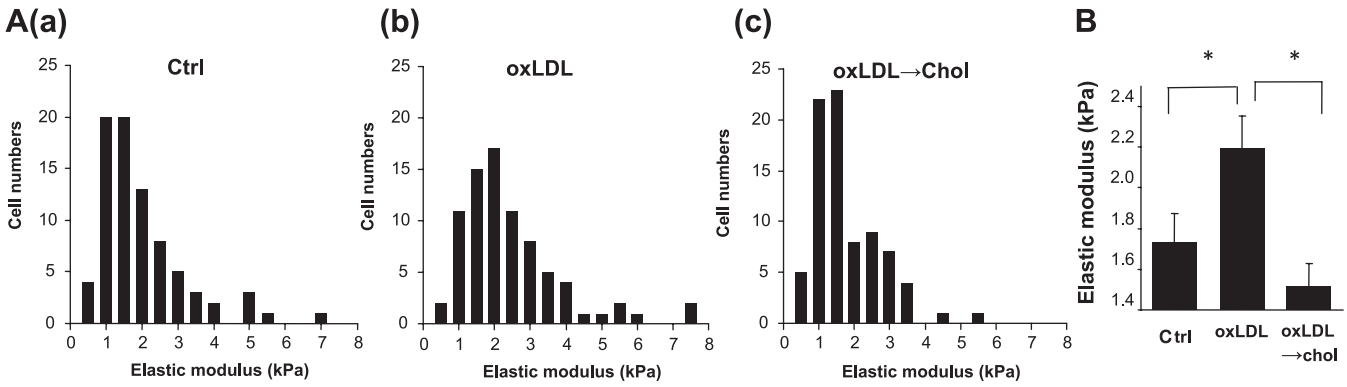

Fig. 3. Cholesterol reverses oxLDL-induced cell stiffening. *Aa–Ac*: histograms of the elastic modulus measured in control cells, 10 μg/mg protein oxLDL-treated cells (oxLDL), and cells treated sequentially with oxLDL and 5 mM MβCD saturated with cholesterol complex (oxLDL→Chol). The data were obtained from 4 independent experiments; all three experimental cell populations were measured in each of the experiments on the same day. *B*: average elastic modulus for Ctrl, oxLDL, and oxLDL→Chol cells. (Data are shown as means ± SE; $n = 80$ cells for each experimental condition. *$P < 0.05$.)

a decrease in the number of cells in the right tail of the distribution (stiff cells). Average values of the elastic modulus under the three experimental conditions are shown in Fig. 3*B*. These observations show that oxLDL-induced effect is fully reversible by supplying the membrane with exogenous cholesterol. Cholesterol enrichment by itself has no effect on endothelial stiffness (Supplemental Fig. S1).

Cell stiffening and disruption of lipid domains by 7-keto-cholesterol and androstenol. To test further whether oxidation of cholesterol itself may be sufficient to induce the same effects on membrane stiffness as oxLDL particles, cells were exposed to 7-keto-cholesterol, a major oxysterol found in oxLDL (13, 28). It has also been shown earlier that incorporation of 7-keto-cholesterol results in a decrease in lipid packing of ordered lipid domains of the liposomes compared with cholesterol (29, 46). Here we show that, similarly to oxLDL, exposing endothelial cells to 7-keto-cholesterol (10 μg/ml for 1 h) results in a significant increase in endothelial elastic modulus, indicating an increase in cell stiffness (Fig. 4, *A* and *B*). Furthermore, we also show that exposure to 7-keto-cholesterol results in a decrease in lipid packing of the ordered domains, as assessed by Laurdan imaging (Fig. 4, *C–E*), an effect that is also very similar to that of oxLDL. More specifically, the peak of the GP values for the ordered domains in 7-keto-cholesterol-treated cells is shifted to significantly lower values, compared with control cells (Fig. 4*E*, red curve: 0.14 ± 0.01 vs. 0.09 ± 0.02 for control and 7-keto-cholesterol-treated cells, respectively; see also Table 2). No significant effect is observed for

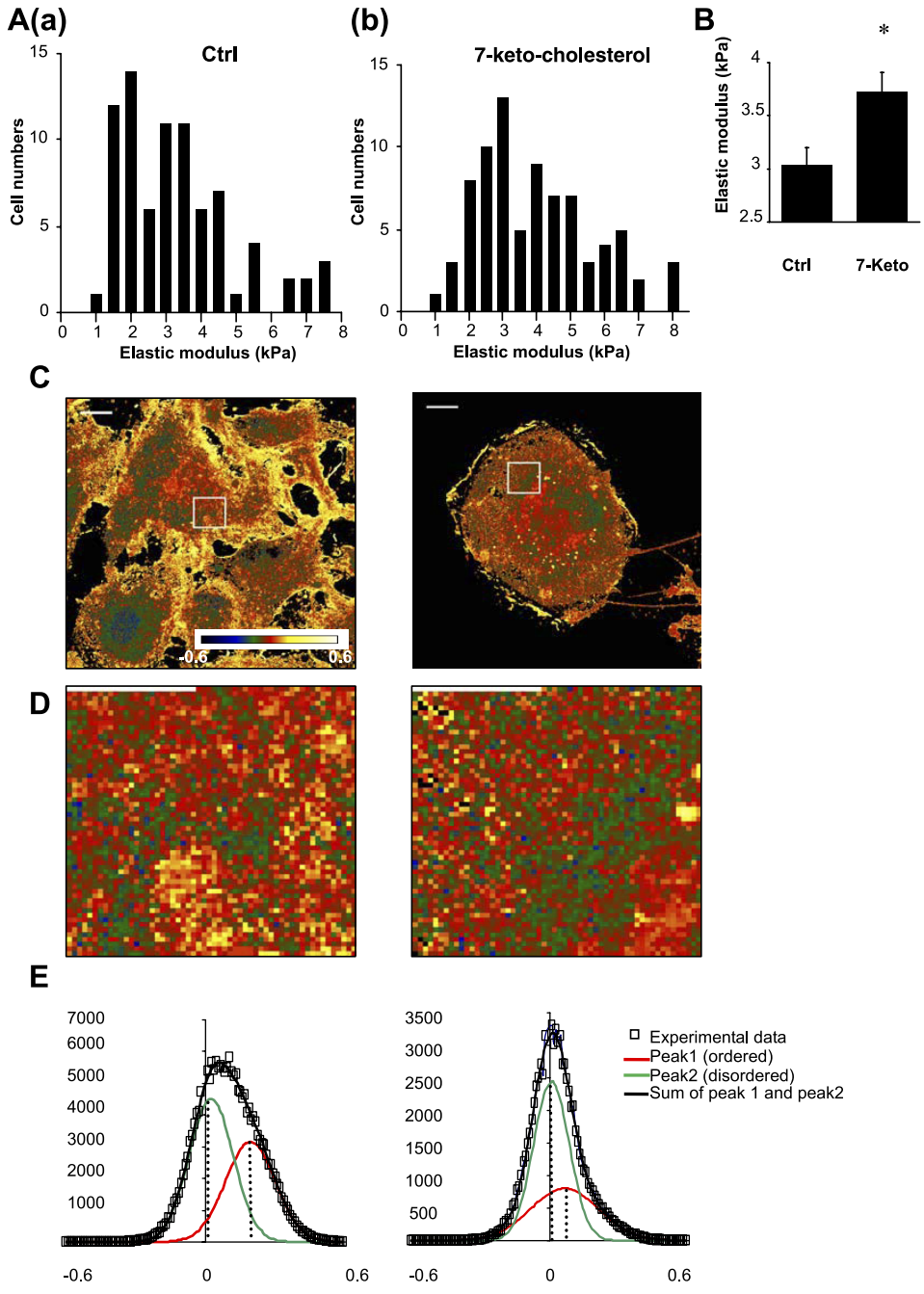

Fig. 4. 7-Keto-cholesterol causes cell stiffening and disorganizes the lipid packing of cholesterol-rich domain. *Aa* and *Ab*: histograms of elastic modulus measured in control and 7-keto-cholesterol-treated cells. *B*: average elastic modulus for control and 7-keto-cholesterol-treated (7-keto) cells. (Values are means ± SE; $n = 80$ cells for each experimental condition. *$P < 0.05$.) *C*: typical GP images of control cells and 7-keto-cholesterol-treated cells. Scale bar is 11.2 μm. *D*: zoom-in representative regions of the GP images shown in *C* (zoomed regions are 11.2 μm × 11.2 μm) Scale bar is 5.6 μm. *E*: GP histograms for the corresponding image fitted by a two-Gaussian distribution with the curve shifted to the *right* representing ordered domains (red) and the curve shifted to the *left* representing fluid domains (green). The sum of the Gaussians is shown in black ($n = 18$ images per experimental condition, 3 independent experiments).

the GP values of the fluid domains, indicating that the effect is specific for the lipid ordered domains only (Fig. 4, *C–E*, and Table 2). The areas of the peaks that represent %membrane coverage are not affected significantly. These observations suggest that cholesterol oxidization is sufficient to induce endothelial stiffening and provide further support for the link between endothelial stiffening and disruption of lipid packing of the membrane.

Furthermore, the inverse correlation between cell stiffening and a decrease in lipid packing is not limited to oxLDL and 7-keto-cholesterol. A significant increase in endothelial elastic modulus is also observed in cells exposed to androstenol (Fig. 5, *A* and *B*), another cholesterol analog that has also been shown to disrupt the formation of lipid ordered domain in the model membrane membranes (47). Also, as expected, exposure to androstenol results in the disruption of lipid packing of lipid ordered domains (Fig. 5, *C–E*, and Table 2), the same effect that was observed for oxLDL and 7-keto-cholesterol.

Sphingomyelin hydrolysis does not affect endothelial elastic properties. Since, as described above, oxLDL is known to activate SMases, we tested whether changes in endothelial biomechanics and network formation may be initiated by sphingomyelin hydrolysis. To test this hypothesis, cells were exposed to bacterial SMase C, a well-established tool to hydrolyze sphingomyelin in mammalian cells (10). Cells were exposed to 0.025 U/ml SMase C, a treatment that was shown

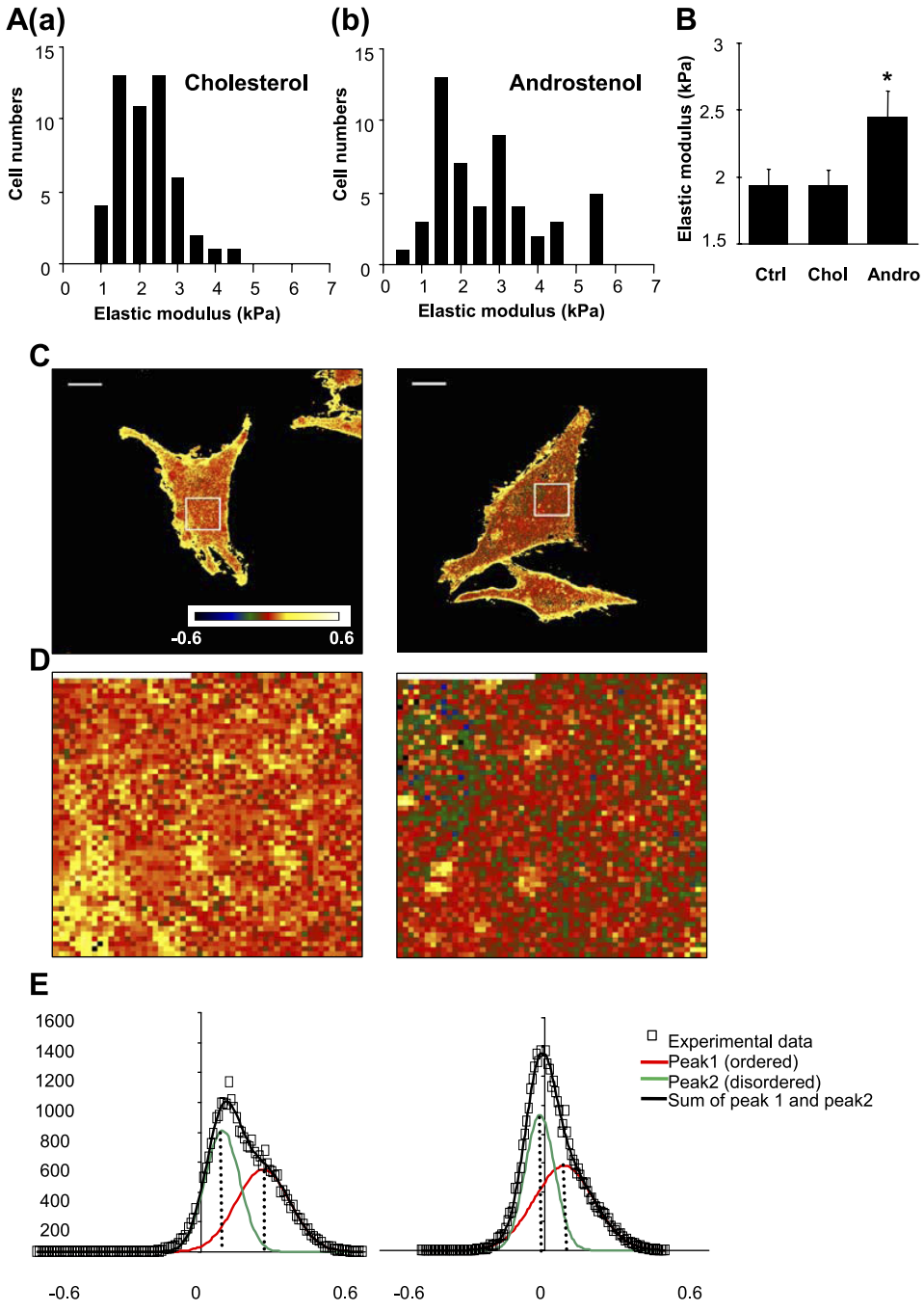

Fig. 5. Androstenol causes the cell stiffening and disorganizes the lipid packing of cholesterol-rich domain. *Aa* and *Ab*: histograms of elastic modulus measured in cells exposed to MβCD-cholesterol or MβCD-androstenol. *B*: average elastic modulus for control (untreated) cells exposed to MβCD-cholesterol (Chol) or MβCD-androstenol (Andro). (Values are means ± SE; $n = 50$ cells for each experimental condition. $^*P < 0.05$.) *C*: typical GP images of cholesterol-treated cells and androstenol-treated cells. Scale bar is 11.2 μm. *D*: zoom-in representative regions of the GP images shown in *C* (zoomed regions are 11.2 μm × 11.2 μm). Scale bar is 5.6 μm. *E*: GP histograms for the corresponding image fitted by a two-Gaussian distribution with the curve shifted to the *right* representing ordered domains (red) and the curve shifted to the *left* representing fluid domains (green).

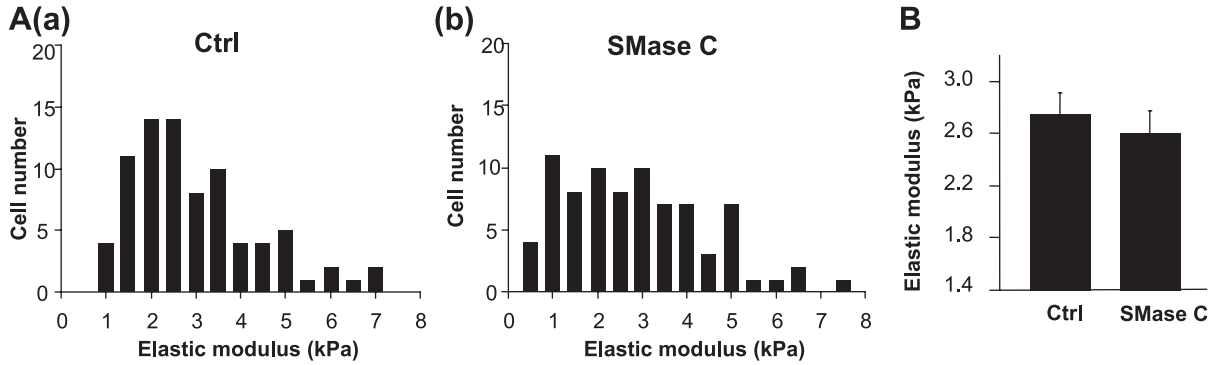

Fig. 6. Hydrolysis of sphingomyelin has no effect on cell stiffening. *Aa* and *Ab*: histograms of elastic modulus measured in control and SMase C-treated cells. *B*: average elastic modulus for control and SMase C-treated cells. (Values are means ± SE; $n = 80$ cells for each experimental condition.)

to decrease membrane sphingomyelin content (38). Indeed, as shown above, treating the cells with SMase C resulted in a significant increase in ACAT activity consistent with a significant decrease in sphingomyelin level (39). However, we show here that exposing BAECs to SMase C had no effect at all on endothelial elastic properties (Fig. 6, *A* and *B*).

Differential effects of cholesterol and sphingomyelin on endothelial contractility. We have also shown earlier that an increase in endothelial stiffness is accompanied with an increase in endothelial force generation as assessed by a gel contraction assay (6). This assay is based on the ability of cells to transmit mechanical forces to the extracellular matrix and contract a malleable 3D gel that the cells are embedded within. In this series of experiments, cells are first exposed to oxLDL or oxLDL/MβCD-cholesterol in serum-free medium, as described in the previous section, and then seeded into a 3D collagen gel in serum containing medium supplemented with the growth factors (50 ng/ml bFGF and 50 ng/ml VEGF) and with 50 ng/ml PMA where cells are maintained for 48 h, time that is required for the cells to elongate and generate an interconnected network (37). Similarly to our earlier study, exposure to oxLDL resulted in a significant decrease in gel diameter, indicating that oxLDL-treated cells are more contractile. Here we show that oxLDL-induced increase in cell contractility is completely reversed by supplying cholesterol surplus (Fig. 7, *A* and *B*). No effect was observed when cells were exposed to MβCD-cholesterol alone (Supplemental Fig. S2, *A* and *B*). Furthermore, we test whether endothelial contractility is also regulated by hydrolysis of sphingomyelin. Our observations show that, in contrast to oxLDL, exposure to SMase C decreases rather than increases cell contractility. These results indicate that oxLDL-induced increase in cell contractility cannot be attributed to hydrolysis of sphingomyelin (Fig. 7, *C* and *D*).

Differential effects of cholesterol and sphingomyelin on EC network formation. It was also shown earlier that the ability of endothelial cells to generate force correlates with their ability to form interconnected endothelial networks in 3D collagen gels (6, 37) an in vitro assay of angiogenesis. Figure 8*A* shows typical examples of endothelial networks of control cells and

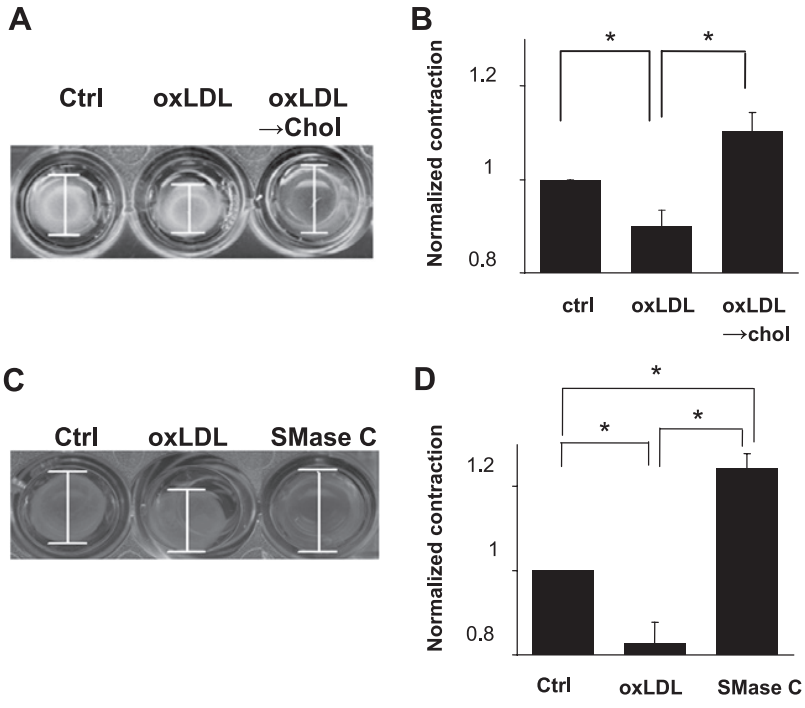

Fig. 7. Differential effects of cholesterol and sphingomyelin on cell contractility. *A*: typical images of collagen gels contracted by Ctrl, oxLDL, or oxLDL→Chol cell populations. *B*: average diameters of the gels 48 h after treatment normalized to control gels in the same experiment. (Values are means ± SE; $n = 7$ independent experiments. *$P < 0.05$.) *C*: typical images of collagen gels contracted by Ctrl, oxLDL, and SMase C-treated cells. *D*: average diameters of the gels 48 h after treatment normalized to control gels in the same experiment. (Values are means ± SE; $n = 3$ independent experiments. *$P < 0.05$.)

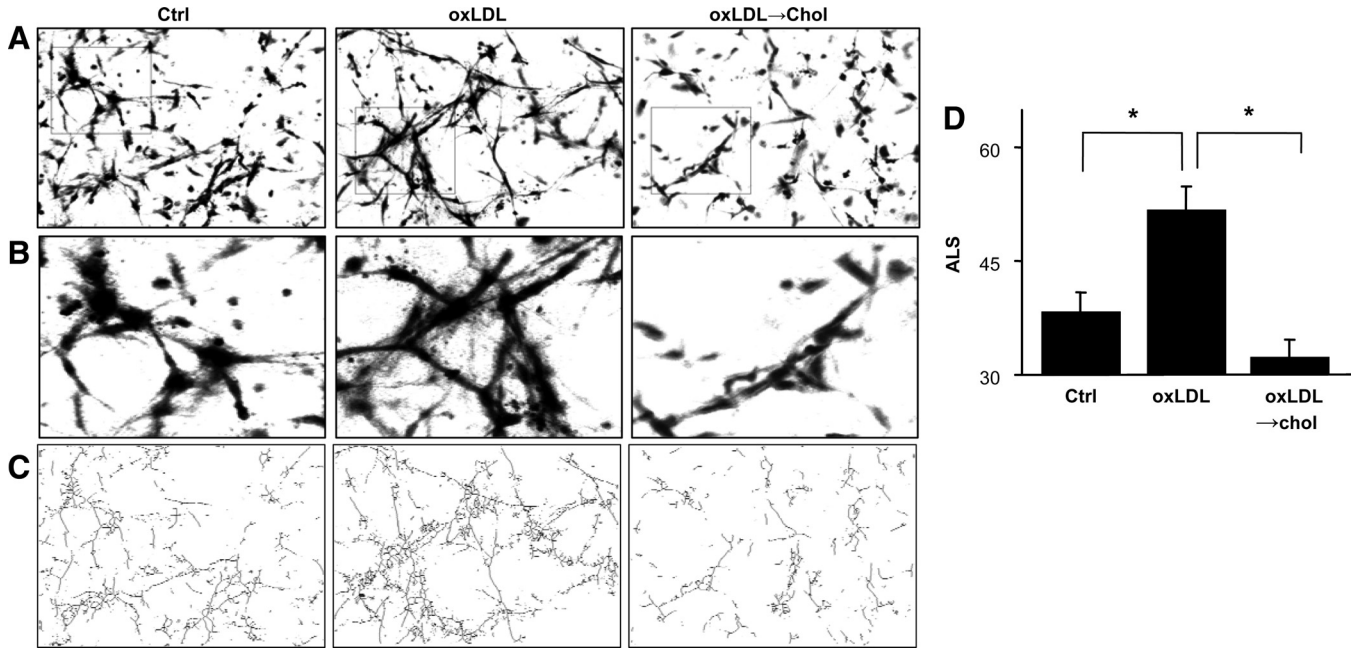

Fig. 8. Cholesterol reverses oxLDL-induced network formation. *A*: images of BAEC networks for Ctrl, oxLDL, and oxLDL→Chol cell populations grown within collagen gels for 48 h. *B*: zoom-in representative regions of the images shown in *A*. *C*: skeletonized versions of the images shown in *A*. *D*: quantification of skeletonized image estimated by average length of skeletonization (ALS). (Values are means ± SE; 50–60 images obtained from 12 different gels for each condition were analyzed in 3 independent experiments. $*P < 0.05$.)

cells exposed to oxLDL or oxLDL/MβCD-cholesterol. As we have shown earlier (6), exposure to oxLDL enhances the ability of endothelial cells to form networks, as apparent from cells being more elongated and forming more connections between them (compare Fig. 8*A*, *left* and *middle*). Most importantly, here we show that sequential exposure to oxLDL and to MβCD-cholesterol results in abrogation of oxLDL-induced effect (Fig. 8, *A–C*, *right*). The zoom in image (Fig. 8*B*) demonstrates that cell-cell connection is more prominent in oxLDL-treated cell population. The difference is quantified by estimating cell length and connectivity in skeletonized images (Fig. 8*C*), as described before (6, 37). An average length of the skeletonized objects (ALS), an index of cell elongation and connectivity for control, oxLDL-, and oxLDL/MβCD-cholesterol-treated cells, is shown in Fig. 8*D*. No effect is observed when cells are exposed to MβCD-cholesterol alone (Supplemental Fig. S2, *C–E*), consistent with a lack of an effect of MβCD-cholesterol on EC elastic modulus and contractility. In contrast, hydrolysis of sphingomyelin has no effect on EC network formation (Fig. 9).

DISCUSSION

A growing number of studies suggest that endothelial biomechanics plays a key role in the control of angiogenesis (6, 18, 22). However, little is known about how endothelial biomechanics is affected by different pathological conditions. Our recent studies have shown that endothelial stiffness is strongly increased in cells exposed to oxLDL, a lipoprotein accumulating in atherosclerotic lesions, as well as in cells isolated from aortas of hypercholesterolemic pigs in diet-induced model of atherosclerosis (6). Furthermore, oxLDL-induced changes in endothelial biomechanics correlate with enhanced endothelial network formation in an in vitro model of angiogenesis (6). In this study, we investigate the mechanism responsible for the impact of oxLDL on endothelial biomechanics and angiogenic potential.

The key question in elucidating the mechanism responsible for oxLDL-induced effects on endothelial biomechanics is to understand what is the relationship between oxLDL, membrane cholesterol, and changes in endothelial elastic properties. Indeed, the impact of oxLDL on the level of membrane cholesterol in endothelial cells has been controversial. Earlier studies proposed that oxLDL is the primary lipoprotein responsible for an increase in cholesterol content in macrophages, but no significant changes were found in endothelial cells (6, 23). Furthermore, Blair et al. (2) showed that oxLDL can actually act as cholesterol acceptor and remove cholesterol from endothelial caveolae. Our previous studies supported this notion indirectly by demonstrating a strong similarity between oxLDL-induced and cholesterol depletion-induced changes in endothelial biomechanics including an increase in endothelial stiffness and sensitivity to flow (5, 24, 40). However, we have found no change in endothelial cholesterol levels in any of the membrane fractions. It is possible, however, that small changes in local levels of membrane cholesterol that are undetectable by biochemical approaches can cause significant changes in local lipid packing. In this study, we test this possibility directly by assessing the local physical properties of the membrane using Laurdan two-photon imaging. Our new data show that oxLDL indeed decreases lipid order of membrane ordered domains, providing a possible mechanistic explanation for the similarities between the impacts of oxLDL and cholesterol depletion on endothelial biomechanics. Furthermore, two additional lines of evidence support our hypothesis that a decrease in membrane order induces endothelial stiffening. First, we show that exposing the cells to 7-keto-cholesterol, a major

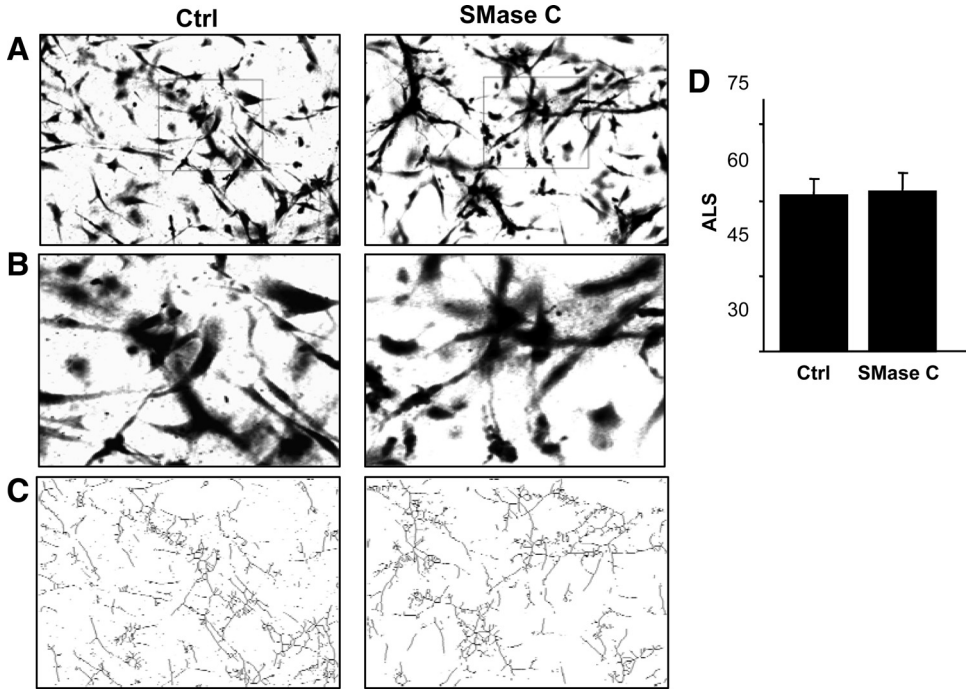

Fig. 9. Hydrolysis of sphingomyelin has no effect on the network formation. *A*: images of BAEC networks for Ctrl and SMase C-treated cell populations grown within collagen gels for 48 h. *B*: zoom-in representative regions of the images shown in *A*. *C*: skeletonized versions of the images shown in *A*. *D*: quantification of skeletonized image estimated by ALS. (Values are means ± SE; 50–60 images, 12 gels per condition, 3 independent experiments.)

oxysterol component of oxLDL (13, 28), results in a decrease in lipid order and an increase in cell stiffness. In addition, the same inverse correlation between the two parameters is observed in cells enriched with androstenol, a sterol known to disrupt lipid packing of the domains (47). In contrast to MβCD, however, that consistent with its ability to extract cholesterol from both ordered and fluid domains (49), decreases the overall membrane order, the effect of oxLDL is specific for the ordered domains only. Similarly, incorporation of 7-keto-cholesterol and of androstenol induces a decrease in lipid packing specifically in lipid ordered domains, further supporting the hypothesis that a decrease in local lipid packing of the ordered domains is responsible for the stiffening effect. These data provide the first insights into the link between oxLDL, membrane order, and endothelial stiffness. Clearly, however, a decrease in lipid packing by itself cannot result in endothelial stiffening, an effect that most likely depends on the properties of the submembrane cytoskeleton, and further studies are needed to elucidate the mechanisms underlying these effects.

The next question that we addressed in this study was whether oxLDL may act as cholesterol acceptor and induce cholesterol efflux or whether it may induce internalization of membrane cholesterol to the intracellular domains. In both cases, a decrease in membrane cholesterol may result in a decrease in lipid order of cholesterol-rich membrane domains. We show here that, indeed, exposure to oxLDL increases cholesterol efflux but has no effect on the internalization of cholesterol. An increase in cholesterol efflux is ~10–20%, but since total cholesterol efflux after 1 h is only a little more than 1% of total membrane cholesterol, it is clearly undetectable when comparing total membrane cholesterol in cells exposed to oxLDL or to the nonoxidized form of LDL. Moreover, it was also undetectable even after biochemical separation of different membrane fractions (6). Our new data, however, demonstrate that small increase in cholesterol efflux is accompanied with significant changes in lipid packing. Taken together, an increase in cholesterol efflux and a decrease in lipid order specifically of the ordered domains suggest that oxLDL acts as cholesterol acceptor removing cholesterol primarily from cholesterol-rich domains of the membrane. Alternatively, it is also possible that oxLDL induces an exchange between native cholesterol of endothelial membrane and oxysterols within the oxLDL complex and that this exchange alters the lipid packing of the membrane. Indeed, it was shown earlier that exposure to oxLDL may enrich cellular membranes with an array of different oxysterols (4). The two possibilities are not mutually exclusive, and both can contribute to alter membrane-cytoskeleton interactions which dominate cellular biomechanical properties.

Finally, we tested whether oxLDL-induced effects on endothelial stiffness, contractility, and network formation are reversed by supplying cholesterol surplus. In this study, endothelial elastic properties are measured using AFM, an approach that allows the measurement of forces with high resolution over a broad range (pN to nN) and which was used to characterize mechanical properties in endothelial cells (30, 35, 36). The values for endothelial elastic modulus obtained in our experiments are in the same range as reported earlier (31, 36) and show a similar increase upon exposure to oxLDL (9). Our new data showing that oxLDL-induced increase in endothelial elastic modulus is fully reversible by a cholesterol donor are a strong indication that cholesterol removal from the membrane is playing an important role in this effect. Furthermore, a similar reversibility of oxLDL-induced effects on endothelial contractility and network formation is further indication that these effects are interrelated and dependent on cholesterol. It is also important to note that changes in cellular elastic modulus in response to oxLDL are similar to changes in membrane elastic moduli under different physiological and pathological conditions (19, 34). Furthermore, similar changes in endothelial stiffness were shown to be associated with a significant

decrease in NO release (35). An increase in endothelial stiffness, therefore, is expected to have a major physiological significance.

How changes in membrane cholesterol may affect cellular biomechanics is not well understood. Several studies have shown that lipid rafts serve as focal points for membrane-cytoskeleton interactions (27). We have also shown recently that cholesterol depletion strengthens the adhesion force between the membrane and the underlying cytoskeleton (40) but has no effect on F-actin stress fibers (5). We suggest, therefore, that endothelial stiffening may be due to changes in actin dynamics, as was suggested by Kwik et al. (25), or due to an increased order of filament cross-linking. Further studies are needed to investigate these possibilities.

In addition to providing insights into the mechanism by which oxLDL alters EC stiffness, force generation and network formation, these results suggest a previously unrecognized link between oxLDL and vascular disease. Since neovascularization of atheromatous lesions is one the major complications of complex lesion formation (8, 44), oxLDL-induced increase in endothelial stiffness and force generation leading to facilitation of angiogenesis may be of critical importance to the progression of atherosclerosis. Remarkably, a link between an increase in endothelial force generation and enhanced angiogenesis was also demonstrated for endothelial cells derived from adenocarcinomas (18), suggesting that this is a general mechanism of control of angiogenesis and underscoring the significance of this mechanism.

ACKNOWLEDGMENTS

The authors thank Dr. Alisha Sieminiski for help with the analysis of networks in the initial stages of this study. We also thank Dr. Gabor Forgacs for comments and suggestions and for the critical reading of the manuscript.

GRANTS

The work was supported by National Heart, Lung, and Blood Institute Grants HL-073965 and HL-083298 (to I. Levitan) and HL-68585 (to P. V. Subbaiah), by National Science Foundation Grant CMMI-0928739 (to K. Gooch), and by American Heart Association predoctoral fellowship 10PRE2570025 (to T. P. Shentu). Atomic Force Microscope was purchased with a grant from the Defense University Research Instrument Program (N00014-04-1-0805 to M. Cho).

DISCLOSURES

No conflicts of interest, financial or otherwise, are declared by the authors.

REFERENCES

1. **Auge N, Maupas-Schwalm F, Elbaz M, Thiers JC, Waysbort A, Itohara S, Krell HW, Salvayre R, Negre-Salvayre A.** Role for matrix metalloproteinase-2 in oxidized low-density lipoprotein-induced activation of the sphingomyelin/ceramide pathway and smooth muscle cell proliferation. *Circulation* 110: 571–578, 2004.
2. **Blair A, Shaul PW, Yuhanna IS, Conrad PA, Smart EJ.** Oxidized low-density lipoprotein displaces endothelial nitric-oxide synthase from plasmalemmal caveolae and impairs eNOS activation. *J Biol Chem* 274: 32512–32519, 1999.
3. **Bollinger CR, Teichgraber V, Gulbins E.** Ceramide-enriched membrane domains. *Biochim Biophys Acta* 1746: 284–294, 2005.
4. **Brown A, Dean R, Jessup W.** Free and esterified oxysterol: formation during copper-oxidation of low density lipoprotein and uptake by macrophages. *J Lipid Res* 37: 320–335, 1996.
5. **Byfield F, Aranda-Aspinoza H, Romanenko VG, Rothblat GH, Levitan I.** Cholesterol depletion increases membrane stiffness of aortic endothelial cells. *Biophys J* 87: 3336–3343, 2004.
6. **Byfield FJ, Tikku S, Rothblat GH, Gooch KJ, Levitan I.** OxLDL increases endothelial stiffness, force generation and network formation. *J Lipid Res* 47: 715–723, 2006.
7. **Cazzolato G, Avogaro P, Bittolo-Bon G.** Characterization of a more electronegatively charged LDL subfraction by ion exchange hplc. *Free Radic Biol Med* 11: 247–253, 1991.
8. **Chen F, Eriksson P, Kimura T, Herzfeld I, Valen G.** Apoptosis and angiogenesis are induced in the unstable coronary atherosclerotic plaque. *Coron Artery Dis* 16: 191–197, 2005.
9. **Chouinard JA, Grenier G, Khalil A, Vermette P.** Oxidized-LDL induce morphological changes and increase stiffness of endothelial cells. *Exp Cell Res* 314: 3007–3016, 2008.
10. **Cremesti AE, Goni FM, Kolesnick R.** Role of sphingomyelinase and ceramide in modulating rafts: do biophysical properties determine biologic outcome? *FEBS Lett* 531: 47–53, 2002.
11. **Dietrich C, Bagatolli LA, Volovyk ZN, Thompson NL, Levi M, Jacobson K, Gratton E.** Lipid rafts reconstituted in model membranes. *Biophys J* 80: 1417–1428, 2001.
12. **Evans E, Needham D.** Physical properties of surfactant bilayer membranes: thermal transition, elasticity, rigidity, cohesion and colloidal interactions. *J Phys Chem* 91: 4219–4228, 1987.
13. **Garcia-Cruset S, Carpenter KL, Guardiola F, Stein BK, Mitchinson MJ.** Oxysterol profiles of normal human arteries, fatty streaks and advanced lesions. *Free Radic Res* 35: 31–41, 2001.
14. **Gardner G, Banka CL, Roberts KA, Mullick AE, Rutledge JC.** Modified LDL-mediated increases in endothelial layer permeability are attenuated with 17β-estradiol. *Arterioscler Thromb Vasc Biol* 19: 854–861, 1999.
15. **Gaus K, Gratton E, Kable EP, Jones AS, Gelissen I, Kritharides L, Jessup W.** Visualizing lipid structure and raft domains in living cells with two-photon microscopy. *Proc Natl Acad Sci USA* 100: 15554–15559, 2003.
16. **Gaus K, Le Lay S, Balasubramanian N, Schwartz MA.** Integrin-mediated adhesion regulates membrane order. *J Cell Biol* 174: 725–734, 2006.
17. **Gaus K, Zech T, Harder T.** Visualizing membrane microdomains by Laurdan 2-photon microscopy. *Mol Membr Biol* 23: 41–48, 2006.
18. **Ghosh K, Thodeti CK, Dudley AC, Mammoto A, Klagsbrun M, Ingber DE.** Tumor-derived endothelial cells exhibit aberrant Rho-mediated mechanosensing and abnormal angiogenesis in vitro. *Proc Natl Acad Sci USA* 105: 11305–11310, 2008.
19. **Hillebrand U, Hausberg M, Stock C, Shahin V, Nikova D, Riethmuller C, Kliche K, Ludwig T, Schillers H, Schneider SW, Oberleithner H.** 17beta-estradiol increases volume, apical surface and elasticity of human endothelium mediated by Na^+/H^+ exchange. *Cardiovasc Res* 69: 916–924, 2006.
20. **Hodis HN, Kramsch DM, Avogaro P, Bittolo-Bon G, Cazzolato G, Hwang J, Peterson H, Sevanian A.** Biochemical and cytotoxic characteristics of an in vivo circulating oxidized low density lipoprotein (LDL−). *J Lipid Res* 35: 669–677, 1994.
21. **Holvoet P, Theilmeier G, Shivalkar B, Flameng W, Collen D.** LDL hypercholesterolemia is associated with accumulation of oxidized LDL, atherosclerotic plaque growth, and compensatory vessel enlargement in coronary arteries of miniature pigs. *Arterioscler Thromb Vasc Biol* 18: 415–422, 1998.
22. **Ingber DE.** mechanical signaling and the cellular response to extracellular matrix in angiogenesis and cardiovascular physiology. *Circ Res* 91: 877–887, 2002.
23. **Jialal I, Chait A.** Differences in the metabolism of oxidatively modified low density lipoprotein and acetylated low density lipoprotein by human endothelial cells: inhibition of cholesterol esterification by oxidatively modified low density lipoprotein. *J Lipid Res* 30: 1561–1568, 1989.
24. **Kowalsky GB, Byfield FJ, Levitan I.** oxLDL facilitates flow-induced realignment of aortic endothelial cells. *Am J Physiol Cell Physiol* 295: C332–C340, 2008.
25. **Kwik J, Boyle S, Fooksman D, Margolis L, Sheetz MP, Edidin M.** Membrane cholesterol, lateral mobility, and the phosphatidylinositol 4,5-bisphosphate-dependent organization of cell actin. *Proc Natl Acad Sci USA* 100: 13964–13969, 2003.
26. **Levitan I, Christian AE, Tulenko TN, Rothblat GH.** Membrane cholesterol content modulates activation of volume-regulated anion current (VRAC) in bovine endothelial cells. *J Gen Physiol* 115: 405–416, 2000.

27. **Levitan I, Gooch KJ.** Lipid rafts in membrane-cytoskeleton interactions and control of cellular biomechanics: actions of oxLDL. *Antioxid Redox Signal* 9: 1519–1534, 2007.
28. **Maor I, Kaplan M, Hayek T, Vaya J, Hoffman A, Aviram M.** Oxidized monocyte-derived macrophages in aortic atherosclerotic lesion from apolipoprotein E-deficient mice and from human carotid artery contain lipid peroxides and oxysterols. *Biochem Biophys Res Commun* 269: 775–780, 2000.
29. **Massey JB, Pownall HJ.** The polar nature of 7-ketocholesterol determines its location within membrane domains and the kinetics of membrane microsolubilization by apolipoprotein A-I. *Biochemistry* 44: 10423–10433, 2005.
30. **Mathur AB, Collinsworth AM, Reichert WM, Kraus WE, Truskey GA.** Endothelial, cardiac muscle and skeletal muscle exhibit different viscous and elastic properties as determined by atomic force microscopy. *J Biomech* 34: 1545–1553, 2001.
31. **Mathur AB, Truskey GA, Reichert WM.** Atomic force and total internal reflection fluorescence microscopy for the study of force transmission in endothelial cells. *Biophys J* 78: 1725–1735, 2000.
32. **Murugesan G, Chisolm GM, Fox PL.** Oxidized low density lipoprotein inhibits the migration of aortic endothelial cells in vitro. *J Cell Biol* 120: 1011–1019, 1993.
33. **Needham D, Nunn RS.** Elastic deformation and failure of lipid bilayer membranes containing cholesterol. *Biophys J* 58: 997–1009, 1990.
34. **Oberleithner H, Riethmuller C, Ludwig T, Shahin V, Stock C, Schwab A, Hausberg M, Kusche K, Schillers H.** Differential action of steroid hormones on human endothelium. *J Cell Sci* 119: 1926–1932, 2006.
35. **Oberleithner H, Riethmuller C, Schillers H, MacGregor GA, de Wardener HE, Hausberg M.** Plasma sodium stiffens vascular endothelium and reduces nitric oxide release. *Proc Natl Acad Sci USA* 104: 16281–16286, 2007.
36. **Ohashi T, Ishii Y, Ishikawa Y, Matsumoto T, Sato M.** Experimental and numerical analyses of local mechanical properties measured by atomic force microscopy for sheared endothelial cells. *Biomed Mater Eng* 12: 319–327, 2002.
37. **Sieminski AL, Hebbel RP, Gooch KJ.** The relative magnitudes of endothelial force generation and matrix stiffness modulate capillary morphogenesis in vitro. *Exp Cell Res* 297: 574–584, 2004.
38. **Subbaiah PV, Billington SJ, Jost BH, Songer JG, Lange Y.** Sphingomyelinase D, a novel probe for cellular sphingomyelin: effects on cholesterol homeostasis in human skin fibroblasts. *J Lipid Res* 44: 1574–1580, 2003.
39. **Subbaiah PV, Sowa JM, Singh DK.** Sphingolipids and cellular cholesterol homeostasis. Effect of ceramide on cholesterol trafficking and HMG CoA reductase activity. *Arch Biochem Biophys* 474: 32–38, 2008.
40. **Sun M, Northup N, Marga F, Byfield FJ, Levitan I, Forgacs G.** Cellular cholesterol effects on membrane-cytoskeleton adhesion. *J Cell Sci* 120: 2223–2231, 2007.
41. **Titushkin I, Cho M.** Modulation of cellular mechanics during osteogenic differentiation of human mesenchymal stem cells. *Biophys J* 93: 3693–3702, 2007.
42. **Van Tits LJ, van Himbergen TM, Lemmers HL, de Graaf J, Stalenhoef AF.** Proportion of oxidized LDL relative to plasma apolipoprotein B does not change during statin therapy in patients with heterozygous familial hypercholesterolemia. *Atherosclerosis* 185: 307–312, 2006.
43. **Vernon RB, Sage EH.** Contraction of fibrillar type I collagen by endothelial cells: a study in vitro. *J Cell Biochem* 60: 185–197, 1996.
44. **Virmani R, Kolodgie FD, Burke AP, Finn AV, Gold HK, Tulenko TN, Wrenn SP, Narula J.** Atherosclerotic plaque progression and vulnerability to rupture: angiogenesis as a source of intraplaque hemorrhage. *Arterioscler Thromb Vasc Biol* 25: 2054–2061, 2005.
45. **Walton KA, Gugiu BG, Thomas M, Basseri RJ, Eliav DR, Salomon RG, Berliner JA.** A role for neutral sphingomyelinase activation in the inhibition of LPS action by phospholipid oxidation products. *J Lipid Res* 47: 1967–1974, 2006.
46. **Wang J, Megha, London E.** Relationship between sterol/steroid structure and participation in ordered lipid domains (lipid rafts): implications for lipid raft structure and function. *Biochemistry* 43: 1010–1018, 2004.
47. **Xu X, London E.** The effect of sterol structure on membrane lipid domains reveals how cholesterol can induce lipid domain formation. *Biochemistry* 39: 843–849, 2000.
48. **Yla-Herttuala S, Palinski W, Rosenfeld ME, Parthasarathy S, Carew TE, Butler S, Witztum JL, Steinberg D.** Evidence for the presence of oxidatively modified low density lipoprotein in atherosclerotic lesions of rabbit and man. *J Clin Invest* 84: 1086–1095, 1989.
49. **Zidovetzki R, Levitan I.** Use of cyclodextrins to manipulate plasma membrane cholesterol content: evidence, misconceptions and control strategies. *Biochim Biophys Acta* 1768: 1311–1324, 2007.